Biosensors and Bioelectronics 100 (2018) 453–461

Contents lists available at ScienceDirect

Biosensors and Bioelectronics

journal homepage: www.elsevier.com/locate/bios

Flexible nanohybrid microelectrode based on carbon fiber wrapped by gold nanoparticles decorated nitrogen doped carbon nanotube arrays: *In situ* electrochemical detection in live cancer cells

Yan Zhang[a], Jian Xiao[a], Yimin Sun[b], Lu Wang[a], Xulin Dong[a], Jinghua Ren[c], Wenshan He[c], Fei Xiao[a,*]

[a] Key laboratory of Material Chemistry for Energy Conversion and Storage, Ministry of Education, Hubei Key Laboratory of Material Chemistry and Service Failure, School of Chemistry and Chemical Engineering, Huazhong University of Science and Technology, Wuhan 430074, PR China
[b] Hubei Key Laboratory of Plasma Chemistry and Advanced Materials, School of Materials Science and Engineering, Wuhan Institute of Technology, Wuhan 430073, PR China
[c] Union Hospital, Tongji Medical College, Huazhong University of Science and Technology, Wuhan 430022, PR China

ARTICLE INFO

Keywords:
Flexible fiber microelectrode
Nitrogen doped carbon nanotube arrays
Gold nanoparticles
Electrochemical biosensors
in situ detection
Cancer cells

ABSTRACT

The rapidly growing demand for *in situ* real-time monitoring of chemical information *in vitro* and *in vivo* has attracted tremendous research efforts into the design and construction of high-performance biosensor devices. Herein, we develop a new type of flexible nanohybrid microelectrode based on carbon fiber wrapped by gold nanoparticles decorated nitrogen-doped carbon nanotube arrays, and explore its practical application in *in situ* electrochemical detection of cancer biomarker H_2O_2 secreted from live cancer cells. Our results demonstrate that carbon fiber material with microscale size and fascinating mechanical properties can be used as a robust and flexible microelectrode substrate in the electrochemical biosensor system. And the highly ordered nitrogen-doped carbon nanotube arrays that grown on carbon fiber possess high surface area-to-volume ratio and abundant active sites, which facilitate the loading of high-density and uniformly dispersed gold nanoparticles on it. Benefited from the unique microstructure and excellent electrocatalytic properties of different components in the nanohybrid fiber microelectrode, an effective electrochemical sensing platform based on it has been built up for the sensitive and selective detection of H_2O_2, the detection limit is calculated to be 50 nM when the signal-to-noise ratio is 3:1, and the linear dynamic range is up to 4.3 mM, with a high sensitivity of 142 μA cm^{-2} mM^{-1}. These good sensing performances, coupled with its intrinsic mechanical flexibility and biocompatibility, allow for its use in *in situ* real-time tracking H_2O_2 secreted from breast cancer cell lines MCF-7 and MBA-MD-231, and evaluating the sensitivity of different cancer cells to chemotherapy or radiotherapy treatments, which hold great promise for clinic application in cancer diagnose and management.

1. Introduction

Cancer is the second largest life-threatening disease that has over 200 types identified all over the world and leads to more than 1500 deaths occurring each day (Jayanthi et al., 2017). In spite of recent technological advancement towards the treatments of cancer, the patient's survival rate is still low due to the poor prognosis and limitation of cancer diagnosis and therapy at the late stage (Pan et al., 2017; Wang et al., 2017). Therefore, early diagnosis of cancer is helpful for its effective treatment and decreasing the mortality rate. However, the conventionally available methods in cancer diagnosis are primarily based on the phenotypic properties of the tumors using ultrasound, X-ray, magnetic resonance imaging, and biopsy (Hossain et al., 2012; Prével et al., 2016; Yang et al., 2017), which are lack of sensitivity for early-stage cancer detection until the cancer cells have spread surrounding tissues and metastasized throughout the body. In recent times, tremendous research efforts have been focused on developing cancer biosensors for their excellent analytical performances in effective measurement of cancer biomarkers to improve the early diagnosis (Jayanthi et al., 2017; Liu et al., 2017a; Mittal et al., 2017). H_2O_2 is a general endogenously enzymatic byproduct of oxidases that plays an increasingly important role in a variety of biological processes and can function as an indicator in tracing many biochemical reactions (Xi et al., 2015; Xiao et al., 2012). Recent researches have demonstrated

* Corresponding author.
E-mail address: xiaofei@hust.edu.cn (F. Xiao).

http://dx.doi.org/10.1016/j.bios.2017.09.038
Received 7 September 2017; Accepted 20 September 2017
Available online 22 September 2017
0956-5663/

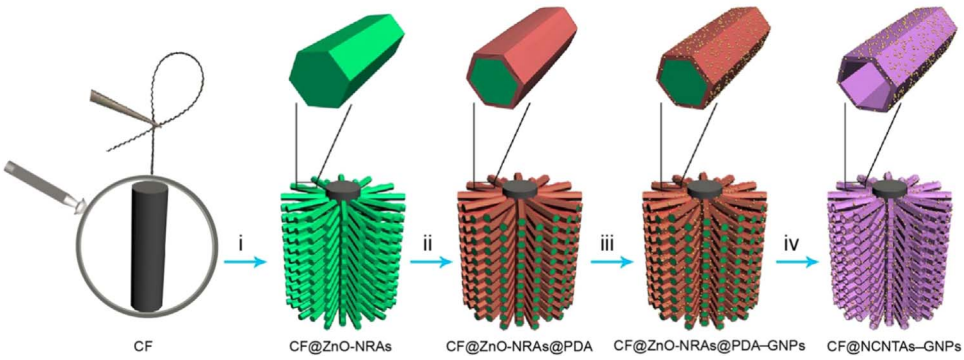

Fig. 1. Schematic illustration of the fabrication procedure of CF@NCNTAs–GNPs nanocomposite. Step i: Growth of ZnO-NRAs on CF *via* hydrothermal process; Step ii Coating PDA layer on ZnO-NRAs *via* polymerization of DA; Step iii: Decorating GNPs on PDA layer *via* chemical reduction of $KAuCl_4$ precursor by catechol groups of PDA. Step iv: Carbonizating and removing ZnO-NRAs template.

that H_2O_2 is excreted by live cells and can reach various cellular regions by diffusing out through the membranes to keep its concentration at the same level (Kim et al., 2017; Lin et al., 2016; Zhu et al., 2016). An appropriate level of H_2O_2 is benefit for body normal function and signal transduction of cells. Nevertheless, it is also noteworthy that the excess of H_2O_2 can destroy the orderliness of the body and lead to different diseases, including Parkinson's, heart attack, Alzheimer's and so on (Bai and Jiang, 2013; Wang et al., 2016a). Especially, emerged evidences have proved that cancer cells can generate more H_2O_2 than normal cells due to an elevation of H_2O_2 production capacity in abnormal growth of tumor (Ju and Chen, 2015; Liu et al., 2015). As a result, H_2O_2 can be used as a specific molecular probe, and the detection of H_2O_2 in biological system is significant for the evaluation of oxidative stress capability distinctions in different live cell as well as the identification of cancer cells.

Nowadays, a wide spectrum of analytical techniques, including spectrophotometry, titrimetry (Liu et al., 2017b), chemiluminescence (Ravi et al., 2003), chromatography (Xu et al., 2016), and electrochemistry (Rui et al., 2010; Sun et al., 2015, 2016; Xi et al., 2016), have been applied for the determination of H_2O_2. Among them, electrochemical methods have sparked great research interests for their explicitly capable in *in situ* real-time analysis of H_2O_2 due to their rapid response, high sensitivity and accuracy, facile operation, user-friendliness, as well as excellent reproducibility (Beitollahi et al., 2014, 2015; Bojdi et al., 2016a, 2014; Karimi-Maleh et al., 2012; Mazloum-Ardakani et al., 2011; Taleat et al., 2008). The electrochemical H_2O_2 sensors are usually based on catalytic redox of H_2O_2 by natural enzyme, *e.g.,* horseradish peroxidase (Chen et al., 2017). However, the inevitable disadvantages, such as complicated immobilization procedure, insufficient stability, and high costs, have seriously limited its application in practice. In comparison with enzymatic sensors, the nonenzymatic H_2O_2 sensors based on noble metals (*e.g.,* Pt, Au, Pd, Ag *etc.)* and their alloy nanoparticles (NPs) have been developed as an alternative for their high specific electrocatalytic activity and outstanding electron transfer ability toward direct electrochemical redox of H_2O_2 (Chen et al., 2012, 2014a; Wang et al., 2016a; Xi et al., 2015; Xiao et al., 2012, 2013; Zhang et al., 2014, 2015). More importantly, loading noble metal NPs on high surface-to-volume ratio support, such as tubular structure, can effectively enhance their electrocatalytic efficiency (Bojdi et al., 2016b; Hosseini et al., 2014), which is anticipated to exhibit good analytical performance in rapid and accurate detection of low-level H_2O_2 in real samples. In parallel with the development of nanocatalyst on electrode, the design of flexible electrode substrates have also attracted tremendous research efforts. In our previous works, several flexible one-dimension (1D), two-dimension (2D) and three-dimension (3D) carbon materials, such as 1D carbon fiber (CF) (Wang et al., 2016), 2D graphene paper (Sun et al., 2015, 2016; Xiao et al., 2013, 2012) and 3D graphene foam (Dong et al., 2015), have been developed in constructing electrochemical biosensors for their special features including high chemical stability, good biocompatibility, and intrinsic flexibility and mechanical strength. Consequently, the resultant modified electrodes exhibit good sensing performances for *in vitro* and *in vivo* tracking biological information.

In this work, we develop a new type of flexible nanohybrid microelectrode based on CF modified by gold nanoparticles (GNPs) decorated highly ordered nitrogen doped carbon nanotube arrays (NCNTAs), and explore its practice application in *in situ* real-time detection of H_2O_2 secreted from live cancer cells. CF is a fascinating flexible substrate in microscale regard due to its small size (5–30 μm in diameter), elasticity modulus, and high tenacity, which can be used in electrical signal transduction of electrochemical biosensor system. In order to increase its active surface area, NCNTAs were directly synthesized on CF by a facile and template-based procedure using ZnO nanorod arrays (NRAs) as the template, where ZnO-NRAs were grown on CF through hydrothermal synthesis and used as the sacrificial template to construct the hollow structure of nitrogen doped carbon (NC), with dopamine (DA) as the carbon source and nitrogen source. DA is a biomolecule that can self-polymerize at alkaline pH values and spontaneously form polydopamine (PDA) films on virtually any surface as well as secondary surface-mediated reaction (Liu et al., 2011; Wang et al., 2016b), and the reduction properties of catechol groups of PDA facilitate the growth of highly dense and well disperse GNPs on the PDA coated support from $KAuCl_4$ precursor. After carbonizating and removing ZnO-NRAs template, the CF wrapped by GNPs decorated NCNTAs (CF@NCNTAs–GNPs) was obtained (Fig. 1). In virtue of the structural merits and electrocatalytic properties of different components in CF@NCNTAs–GNPs, a highly sensitive, selective and reliable sensing platform has be built up for nonenzymatic electrochemical detection of H_2O_2 and *in situ* real-time tracking H_2O_2 secreted from breast cancer cell lines MCF-7 and MBA-MD-231. The results show that the proposed electrochemical sensor based on flexible CF@NCNTAs–GNPs microelectrode can determine H_2O_2 secreted from MDA-MB-231 and MCF-7 cells stimulated by extracellular matters, and evaluate the sensitivity of different cancer cells to chemotherapy or radiotherapy treatments, which is of great clinic significance for the development of effective strategies in the diagnosis and treatment of different cancer diseases.

2. Material and methods

2.1. Reagents and apparatus

Zinc acetate, ethylenediamine, ethylene glycol methyl ether, zinc nitrate hexahydrate and hexamethylene tetramine were purchased from Aladdin Chemistry Co., Ltd (China) and have been used for the preparation of ZnO-NRAs. DA, $KAuCl_4$, tris(hydroxymethyl) aminomethane and HCl (mass fraction is 37.5%) were obtained from Sigma-Aldrich Co., Ltd (USA). Ascorbic acid (AA), β-D(+)-glucose, uric acid (UA), and H_2O_2 were obtained from Sinopharm Chemical Reagent Co., Ltd (China). N-formylmethionyl-leucyl-phenyl-alanine (fLMP, ≥99.5%) and catalase (come from bovine liver, Lyophilized, ≥ 3000 units mg^{-1}) were obtained from Sigma-Aldrich Co., Ltd (USA). Dulbecco's modified eagle's medium (DMEM), fetal bovine serum (FBS), trypsine-EDTA

(0.25%) and penicillinstreptomycin were purchased from HyCl one (Waltham, USA). The chemotherapeutic agent cisplatin (DDP), propidium iodide (PI) and calcein AM viability dye (UltraPure Grade) were purchased from Sigma (USA). All other chemicals used were of analytical reagent grade. All solutions were prepared using deionized water (resistivity: 18.25 Ω cm^{-1}). All these chemicals were of reagent grade and have been used to prepare solutions with doubly distilled water. 0.1 M phosphate buffer saline (PBS, pH 7.4) solution consisting of KH_2PO_4 and K_2HPO_4 was used as the electrolyte for electrochemical experiments and physiological environment for cell testing. All of the mentioned solutions were prepared with deionized water.

2.2. Preparation of CF@NCNTAs–GNPs nanocomposite

For the fabrication of flexible CF@NCNTAs–GNPs microelectrode, a bundle of CF was soaked in 30% H_2O_2 in the oven for 6 h, and then it was washed by deionized water and acted as a substrate for the growth of ZnO-NRAs by the hydrothermal process. In detail, CF was placed in 40 mL teflon reactor with 50 mM zinc nitrate hexahydrate and 50 mM hexamethylene tetramine mixed solutions with a seed layer, and the seed layer was obtained from the solution of 4 mM zinc acetate-ethylene glycol methyl ether. After that, the teflon reactor was heated at 90 °C for 12 h in an oven. The obtained product of ZnO-NRAs wrapped CF (CF@ZnO-NRAs) was washed with deionized water and dried in the air. Subsequently, 100 mg of DA was dissolved in 50 mL Tris-buffer (pH 8.5) by ultrasonication for 10 min and then added with the CF@ZnO-NRAs. After 10 h, PDA film was coated on the surface of ZnO-NRAs. Then, 2 mM $KAuCl_4$ was added into the above suspension and reacted for 15 min under the ice-bath condition. The resultant GNPs decorated CF@ZnO-NRAs@PDA (CF@ZnO-NRAs@PDA–GNPs) was washed with deionized water for three times, and dried by freeze-drying. The obtained sample was heated at 500 °C in a quartz tube under Ar atmosphere with a heating rate of 10 °C min^{-1} for 2 h to transfer PDA layer into NC layer wrapped ZnO-NRAs. Finally, the prepared product was soaked in 0.1 M HCl solution for 1 h to remove ZnO-NRAs template and being freeze-dried, and CF@NCNTAs–GNPs was obtained.

2.3. Characterization

The scanning electron microscope (SEM, Zeiss, Germany) and high-resolution transmission electron microscopy (HRTEM, TECNAI G220 U-Twin instrument, Netherlands) were employed for the characterization of morphologies and surface structures. X-ray photoelectron spectroscopy (XPS) experiments were measured on an ESCALAB MKII spectrometer (VG Co., U.K.) to examine the relevant composition. The X-ray diffraction (XRD) analyses were performed using a Rigaku diffractometer model Multiflex with a CuKα radiation source to investigate the crystal structures. The fluorescence microscope (Olympus BX41F, Japan) equipped with a DP73 camera was used to examine cells statues under light with the different wavelengths. The images were taken with the software cellSens standard 1.7 (Olympus, Japan). The radiation treatment was performed with 6 MV X-ray linear accelerator (Primus, Siemens AG, Erlangen, Germany). Cyclic voltammetric (CV) and chronoamperometric experiments were performed with the CHI660E electrochemical workstation (CH Instrument Company, Shanghai, China) using a conventional three-electrode system. The working electrode is the flexible nanohybrid fiber microelectrode, the reference electrode is Ag/AgCl electrode, and the counter electrode is a platinum wire. All potentials were measured and reported *versus* the Ag/AgCl electrode. All electrochemical tests were carried out in 0.1 M PBS solution (pH 7.4) with stirring. And the tested solution was ventilated with high-purity nitrogen to exclude the interference of oxygen.

2.4. Cell culture

The breast cancer cells MCF-7 and MBA-MD-231 were seeded at a density of 10^5 cells/well into 6-well plates and maintained in a culture medium consisting of DMEM at 37 °C, and subcultured every 3 days. Calcein-AM viability dye was dissolved in dimethyl sulphoxide (DMSO), and the concentration is 1 mM. PI was dissolved in ddH_2O, and the concentration is 1.5 mM. The calcein-AM and PI solutions were stored at −20 °C. The dye solution was prepared by mixing 10 μL calcein-AM and 15 μL PI solutions with 5 mL PBS solution, the final concentrations of calcein-AM and PI are 2 μM and 4.5 μM, respectively. To assess cell viability, 100 μL dye solution was added into 200 μL washed cells suspension (10^5–10^6/mL), which was incubated for 15 min at 37 °C to stain viable cells green and dead cells red. The samples were then rinsed twice in PBS solution and observed by a fluorescent microscope. Cell number was calculated by using a cell counter. For chemotherapy, the cells were treated with DDP (0.01 M, pH 7.4) with a final concentration of 0.2 μg mL^{-1}. And after 24 h, serum-free DMEM containing CFSE (2.5 μM) was added into each well. For radiation treatment, the cells were irradiated using a 6 MV X-ray linear accelerator at a dose rate of 200 cGy/min using a collimator with a 40 × 40 cm^2 radiation field at the treatment isocenter. The dose of radiation was 2 Gy. For electrochemical experiments, CF@NCNAs–GNPs was acted as the working electrode and placed near the live cells in testing solution containing 5.0 × 10^6 cells, fLMP was injected into the cells to stimulate live cells to generate H_2O_2, and the current responses were recorded by CHI 660E.

3. Results and discussion

3.1. Structural and compositional characterization of CF@NCNTAs–GNPs nanocomposite

The morphologies of the as-prepared nanohybrid fibers with different magnifications are presented in Fig. 2. CF with a typical diameter of 10 μm and length of 2 cm (Fig. 2A and B), was activated by H_2O_2 and used as the electrode substrate. The preparation procedure of CF@NCNTAs–GNPs involves three steps. First, the freestanding ZnO-NRAs have grown on CF *via* a hydrothermal synthesis method. During this procedure, the surface of CF is entirely wrapped by close-packed ZnO nanorods (Fig. 2C and D), which are vertically grown on the surface of CF to form array structure (Fig. 2E). From the higher-magnification SEM image, it can be observed that individual ZnO nanorod exhibits a well-defined hexagonal prism shape and smooth side facets, with homogeneous diameter of less than 100 nm and average length of 2 μm (Fig. 2F). Second, ZnO-NRAs on CF are uniformly covered with PDA film *via* polymerization of DA, followed by decorated with GNPs through chemical reduction of their precursor solution by catechol groups of PDA. Finally, after carbonizating and removing ZnO-NRAs template, PDA coated ZnO-NRAs were converted to highly ordered NCNTAs (Fig. 2G), where GNPs are decorated on the shell of the nanotubes (Fig. 2H). Fig. 2I shows the TEM image of several GNPs decorated carbon nanotubes peeled off from CF substrate under the ultrasonication assistance, which reveals the typical hollow structure of N-doped carbon nanotubes after removing the ZnO nanorods template, and the GNPs with uniform size and high density are well distributed on the surface of nanotubes. The high-resolution TEM (HRTEM) image shown in Fig. 2J demonstrates that the amorphous carbon shell of nanotubes is ~ 7 nm, and the average size of GNPs decorated on the carbon nanotubes is ~ 5 nm. The lattice spacing of 0.24 nm for GNP is corresponding to (111) lattice planes of Au specie (Fig. 2K) (Chen et al., 2014b; Thanh et al., 2016). The element distribution in CF@NCNTAs–GNPs has been shown by SEM mapping, which exhibits the uniform and intensive distribution of C, N and Au elements in the nanohybrid fiber (Fig. 2L), indicative of the successful synthesis of NCNTAs and effective decoration of GNPs on their surface.

The XPS characterization has been performed to investigate the surface chemical composition of CF@NCNTAs–GNPs, which presents four main peaks assigned to Au 4f C 1s, N 1s and O 1s (Fig. 3A). From

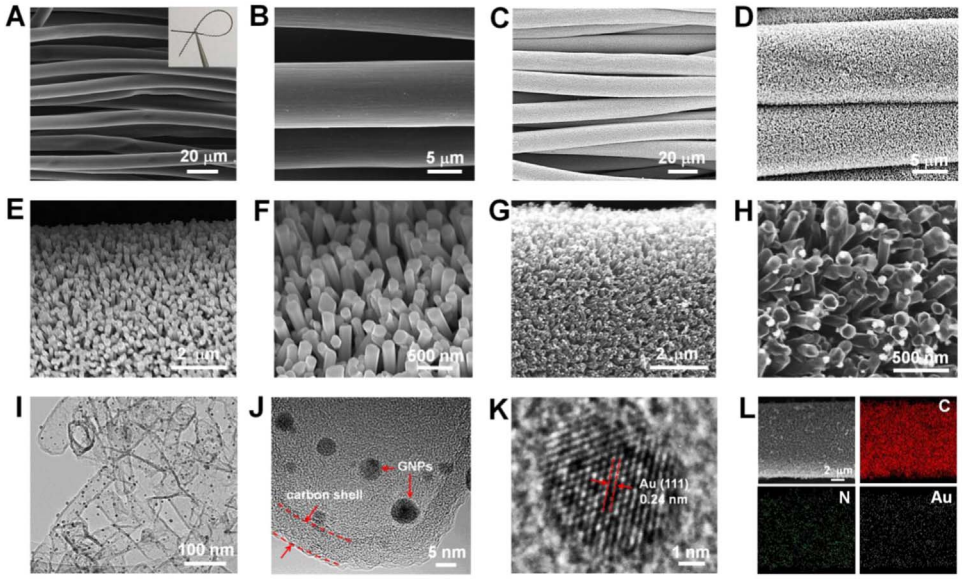

Fig. 2. SEM images of (A) and (B) CFs, (C)-(F) CF@ZnO-NRAs, (G) and (H) CF@NCNTAs–GNPs nanocomposite with different magnifications. Inset of (A) is the digital photograph of CF. (I) TEM image of several GNPs decorated nitrogen doped carbon nanotubes peeled off from CF substrate. HRTEM image of (J) a single nitrogen doped carbon nanotube and (K) GNP decorated on it. (L) Scanning elemental mapping of CF@NCNTAs–GNPs nanocomposite.

the high resolution C 1s XPS spectrum, it can be seen that the C 1s region can be convoluted into three main contributions, *i. e.,* the peak at 285.0 eV belongs to sp^2-hybridized graphite-like carbon (C-C sp^2), the peak at 286.4 eV assigns to C-N, and the peak at 288.4 eV originates from O=C-O groups (Fig. 3B) (Yu et al., 2014). The XPS spectrum of N 1s can be divided into three main peaks. The peaks at 398.7 eV, 400.0 eV and 401.5 eV are featured as pyridinic nitrogen, pyrrolic nitrogen and quaternary nitrogen groups, respectively, demonstrating that PDA layer was converted to NC layer after carbonization, which is anticipated to favor the cation transport on the surface electrode material for defects in the carbon shell caused by N doping (Fig. 3C) (Balamurugan et al., 2017; Xi et al., 2016). Furthermore, the high resolution Au 4 f XPS spectrum displays two doublets at 84.1 eV and 87.8 eV (Fig. 3D), which are consistent with the previous report for GNPs (Zhuang et al., 2014).

Fig. 3E displays the XRD profiles of CF@ZnO-NRAs, CF@ZnO-NRAs@NC, CF@ZnO-NRAs@NC–GNPs and CF@NCNTAs–GNPs. All of the nanohybrid fibers show a weak and broad peak at 26° corresponding to graphitic planes of CF (Paul et al., 2017). For CF@ZnO-NRAs, CF@ZnO-NRAs@NC and CF@ZnO-NRAs@NC–GNPs, there are seven diffraction peaks corresponding to the (100), (002), (101), (102), (110), (103) and (112) facets of ZnO (JCPDS 036-1451) (Fang et al., 2017). Moreover, the XRD pattern of CF@NCNTAs–GNPs indicates that the diffraction peaks located at 38.23°, 44.48°, 64.74° and 77.73°, assigning to the (111), (200), (220) and (311) facts of Au species (JCPDS 00-001-1172) (Zhong et al., 2017) of GNPs in the nanocomposite. After removing the ZnO-NRAs template, all the diffraction peaks corresponding ZnO disappear, only diffraction peaks that corresponding to C and Au species are observed, confirming the formation of NCNTAs decorated by GNPs.

3.2. Electrochemical characterization of CF@ZnO@NCNTAs–GNPs microelectrode

The CV technique has been applied to investigate the electrochemical properties of different nanohybrid fiber microelectrodes using $[Fe(CN)_6]^{3-/4-}$ as a redox probe (Fig. 3F). The CV curve of bare CF microelectrode demonstrates a pair of quasi-reversible redox peaks of $[Fe(CN)_6]^{3-/4-}$ couple, but the peak current density (j_p) is small and the peak potential separation (ΔE_p) is large due to the low electro-activity and weak wettability of unmodified CF. When bare CF has been modified by a layer of NCNTAs, the j_p value of redox waves associated with $[Fe(CN)_6]^{3-/4-}$ probe exhibits an obvious increment in comparison with that of bare CF, and the ΔE_p value decreases as well, illustrating that the NCNTAs layer on CF has provided necessary conduction pathways in promoting the electron transfer of ferricyanide ions. CF@NCNTAs microelectrode with large surface area and abundant active sites serves as an ideal substrate to load electroactive nanomaterials. After being decorated by GNPs, the CV curve of CF@NCNTAs–GNPs microelectrode demonstrates remarkable decrease of ΔE_p value and increase of j_p value. The electrochemically active surface area (ECSA) values of different microelectrodes have been estimated according to the slope of the i_p *versus* $v^{1/2}$ plot based on the Randles-Sevcik equation, the ECSA value of CF@NCNTAs–GNPs microelectrode is 2-fold higher than that of CF@NCNTAs microelectrode, and 7-fold higher than that of bare CF microelectrode, indicating that the loading of GNPs on NCNTAs has accelerated the heterogeneous electron transfer between the electrode and the $[Fe(CN)_6]^{3-/4-}$ redox species, and dramatically increased ECSA of CF@NCNTAs–GNPs microelectrode.

3.3. Electrochemical sensing performance of CF@NCNTAs–GNPs microelectrode to H_2O_2

The developed CF@NCNTAs–GNPs microelectrode has been used in electrochemical detection of H_2O_2 under the optimized condition, with bare CF microelectrode and CF@NCNTAs microelectrode as the control. As shown in CV curves of Fig. 4A, the current response of bare CF microelectrode toward 4 mM H_2O_2 is negligible. While for CF@NCNTAs microelectrode, a distinct H_2O_2 reduction peak can be observed at −0.6 V. Compared to CF@NCNTAs microelectrode, the j_p of H_2O_2 reduction on CF@NCNTAs–GNPs microelectrode dramatically increased, and the peak potential shifts to −0.3 V. Furthermore, the current responses substantially enhance with the successive increase of H_2O_2 concentration (Fig. 4B). The high electrocatalytic behavior of CF@NCNTAs–GNPs microelectrode toward H_2O_2 should be attributed to the synergistic effect of unique structure of NCNTAs and highly electrocatalytic activity of GNPs on them, which offer numerous electrocatalytically active sites for redox reaction of H_2O_2 and high electric conductivity to promote the electron transport on the electrode/electrolyte interface.

Fig. 4C shows the amperometric responses of CF@NCNTAs–GNPs microelectrode to the aliquot addition of different concentrations of H_2O_2 in continuously stirred the reaction solution at an operational potential of −0.3 V. With the successive additions of H_2O_2, well-defined steady-state amperometric current responses are obtained within 3 s, and the current densities increase stepwise. From the linear relationship between the corresponding current densities and the H_2O_2

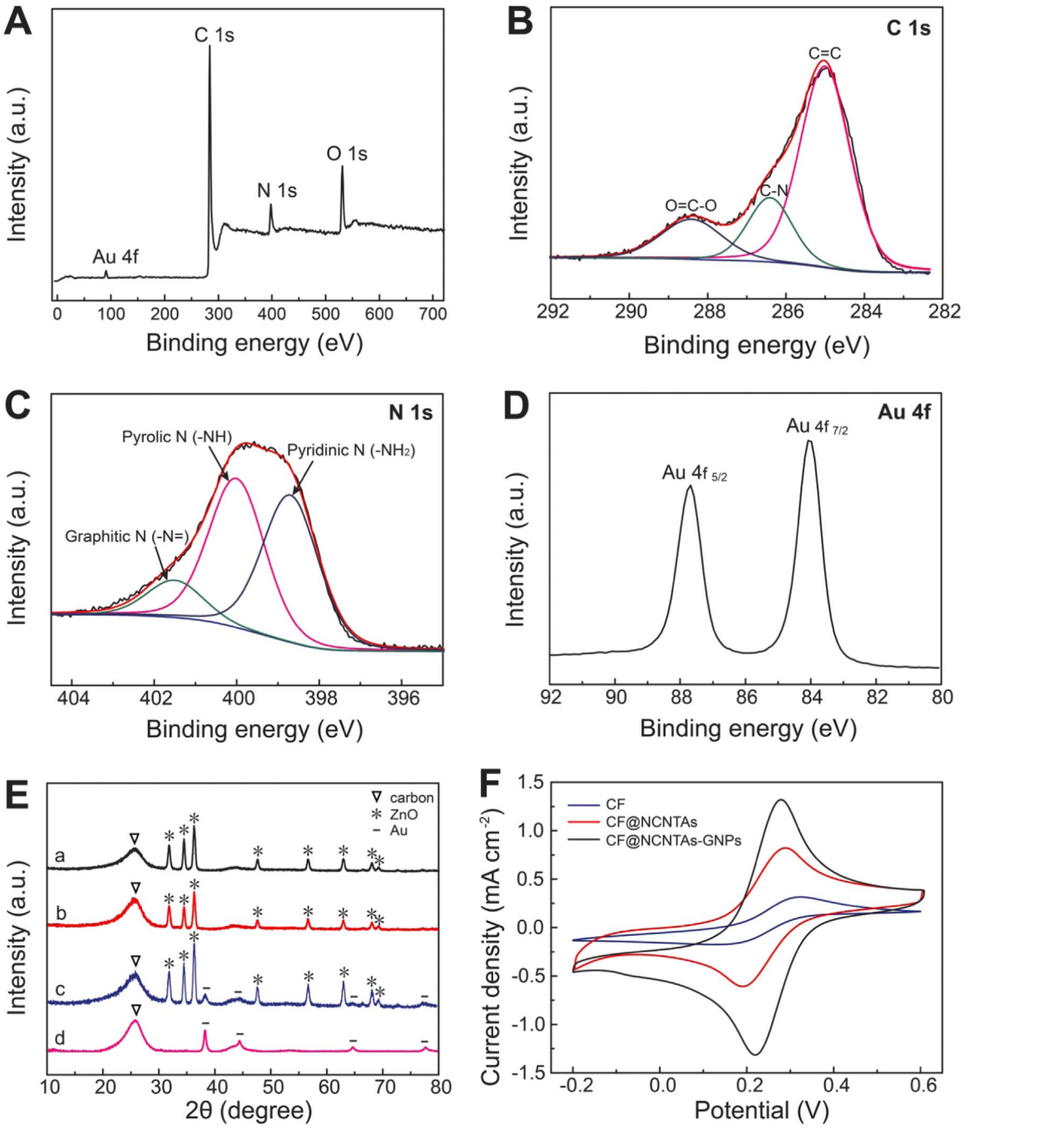

Fig. 3. (A) XPS survey spectrum of CF@NCNTAs–GNPs, and curve fit of (B) C 1s, (C) N 1s, and (D) Au 4f spectra of CF@NCNTAs–GNPs. (E) XRD patterns of CF@ZnO-NRAs (a), CF@ZnO-NRAs@PDA (b), CF@ZnO-NRAs@PDA–GNPs (c) and CF@NCNTAs–GNPs (d). (F) CV curves of bare CF, CF@NCNA and CF@NCNTAs–GNPs microelectrodes in 0.1 M KCl containing 1.0 mM $K_3Fe(CN)_6$ and 1.0 mM $K_4Fe(CN)_6$, scan rate: 50 mV s^{-1}.

concentrations shown in Fig. 4D, the detection limit is calculated to be 50 nM when the signal-to-noise ratio is 3:1 (S/N = 3), and the current density displays an expanded linear relationship with the H_2O_2 concentrations increasing to 4.3 mM, and the sensitivity is 142 μA cm^{-2} mM^{-1}. These performances are superior to those of the previous reported nonenzymatic nanohybrid electrodes (Supplementary material, Table S1).

The sensing performances with respect to selectivity, reproducibility, and stability are investigated in detail. As displayed in Fig. 4D inset, ten different CF@NCNTAs–GNPs microelectrodes tested by amperometric measurement provide a relative standard deviation (R.S.D.) value of 4.6% for 200 μM H_2O_2. And one CF@NCNTAs–GNPs microelectrode exhibits a low R.S.D. value of 4.4% for ten repetitive amperometric testing of 200 μM H_2O_2. The stability of CF@NCNTAs–GNPs microelectrode has been estimated by measuring its amperomatric current response to 200 μM H_2O_2 after 30 days storage, and the current density retains 92.7% of its initial value. These indicate the good reproducibility, repeatability and stability of the proposed nanohybrid fiber microelectrode. The anti-interference ability of the CF@NCNTAs–GNPs microelectrode was measured by injecting several electroactive species such as ascorbic acid (AA), uric acid (UA), dopamine (DA), and glucose (GLU) into a certain amount of H_2O_2. The results show that the addition of 2 mM DA, UA, AA and GLU have no influence on amperomatric response of 100 μM or 200 μM H_2O_2 (Fig. S1). Therefore, the CF@NCNTAs–GNPs microelectrode displays good selectivity at the operational working potential of −0.3 V.

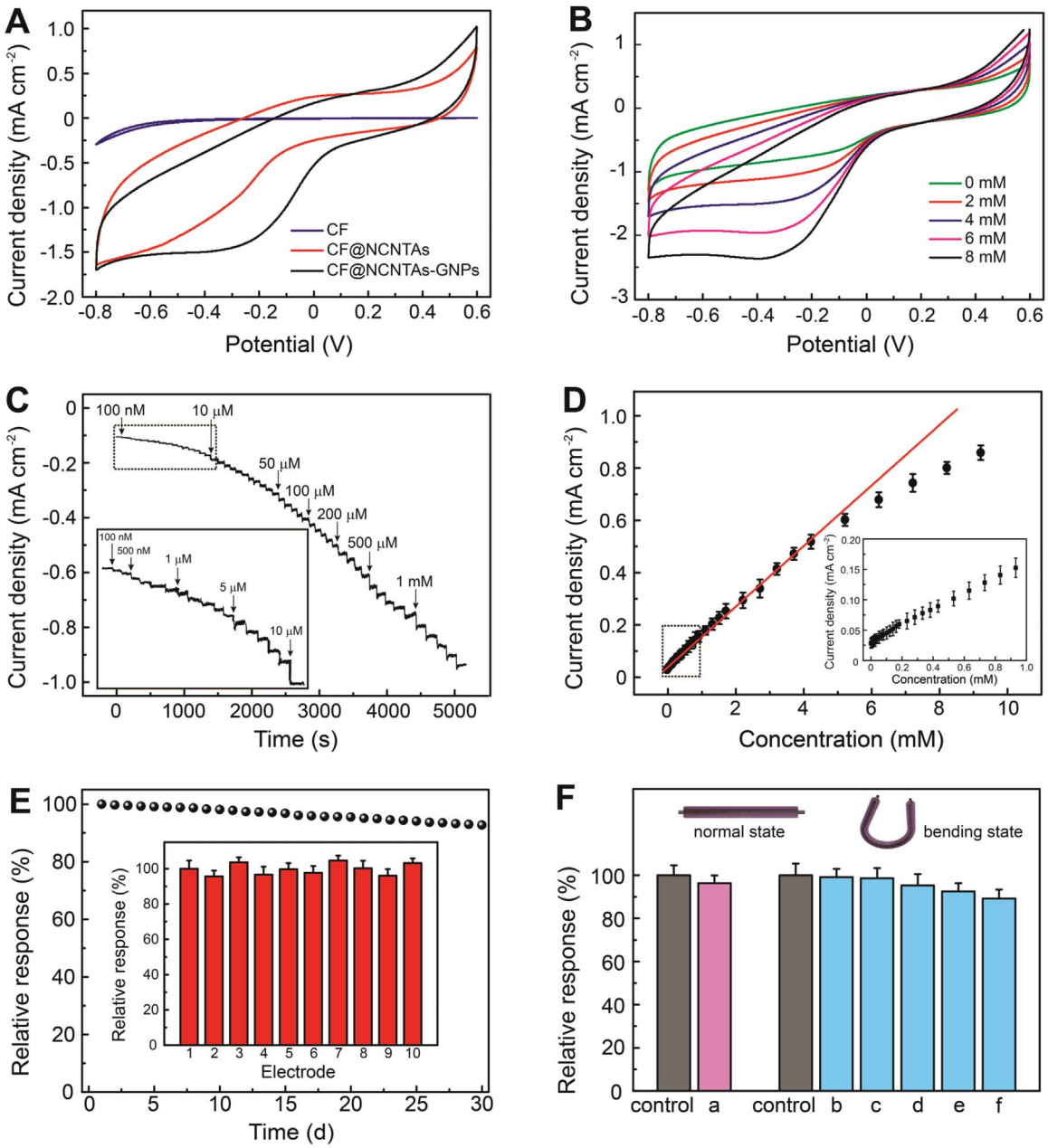

Fig. 4. (A) CV curves of CF, CF@NCNTAs and CF@ NCNTAs–GNPs microelectrodes in 0.1 M PBS solution (pH 7.4) containing 4 mM H_2O_2. (B) CV curves of CF@NCNTAs-GNPs electrode in 0.1 M PBS solution (pH 7.4) containing 0, 2, 4, 6 and 8 mM H_2O_2, scan rate 50 mV s^{-1}. (C) Amperometric *j*-t responses of CF@NCNTAs–GNPs microelectrode to the addition of different H_2O_2 concentration into 0.1 M PBS (pH 7.4) under stirring, applied potential: −0.3 V. Inset of (C) is the amperometric response of low concentrations of H_2O_2. (D) The calibration curves of linear relationship between the corresponding current densities and the H_2O_2 concentrations. (E) Effect of bending states on the amperometric responses of 10 μM H_2O_2: in normal state (control), in bending state (a), and after repetitive bending of 100 (b), 200 (c), 300 (d), 400 (e) and 500 (f) times.

For flexible fiber based microelectrodes, their electrochemical performance should be maintained almost constant under the different bending states. Herein, the amperometric measurements were conducted to investigate mechanical stability of the flexible CF@NCNTAs–GNPs microelectrode at different bending angles. Remarkably, the amperometric response of 200 μM H_2O_2 on CF@NCNTAs–GNPs microelectrode at bending state is 96.3% of that at normal state. Furthermore, when the fiber microelectrode is upon repetitive bent for 500 times, the amperometric response remains 89.2% of its initial value (Fig. 4F). These indicate that its electrocatalytic performance is not affected by the bending induced mechanical stress. The good mechanical stability is owing to the high toughness and stiffness of CF substrate and good adhesion of NCNTAs and GNPs grown on it. These unique structural and mechanical properties are beneficial to roll up the flexible fiber microelectrode for wearable or implantable biomedical devices.

3.4. *In situ real-time tracking of H_2O_2 secreted from live cancer cells*

The proposed CF@NCNTAs–GNPs microelectrode has further been used in *in situ* real-time detection of H_2O_2 released from two types of breast cancer cells, *i.e.,* MCF-7 cells and MDA-MB-231 cells. At first, the cytotoxicity of CF@NCNTAs–GNPs to live cells has been investigated by dual-fluorescent calceinAM/PI assay and standard cell counting Kit-8 (CCK-8) assay. Fig. 5A-D display the dark-field fluorescent images of MCF-7 cells and HBL-100 cells incubated with CF@NCNTAs–GNPs and stained by calcein AM/PI, revealing that these live cells are health when incubated with CF@NCNTAs–GNPs for 4 h, with a high live-to-dead cell

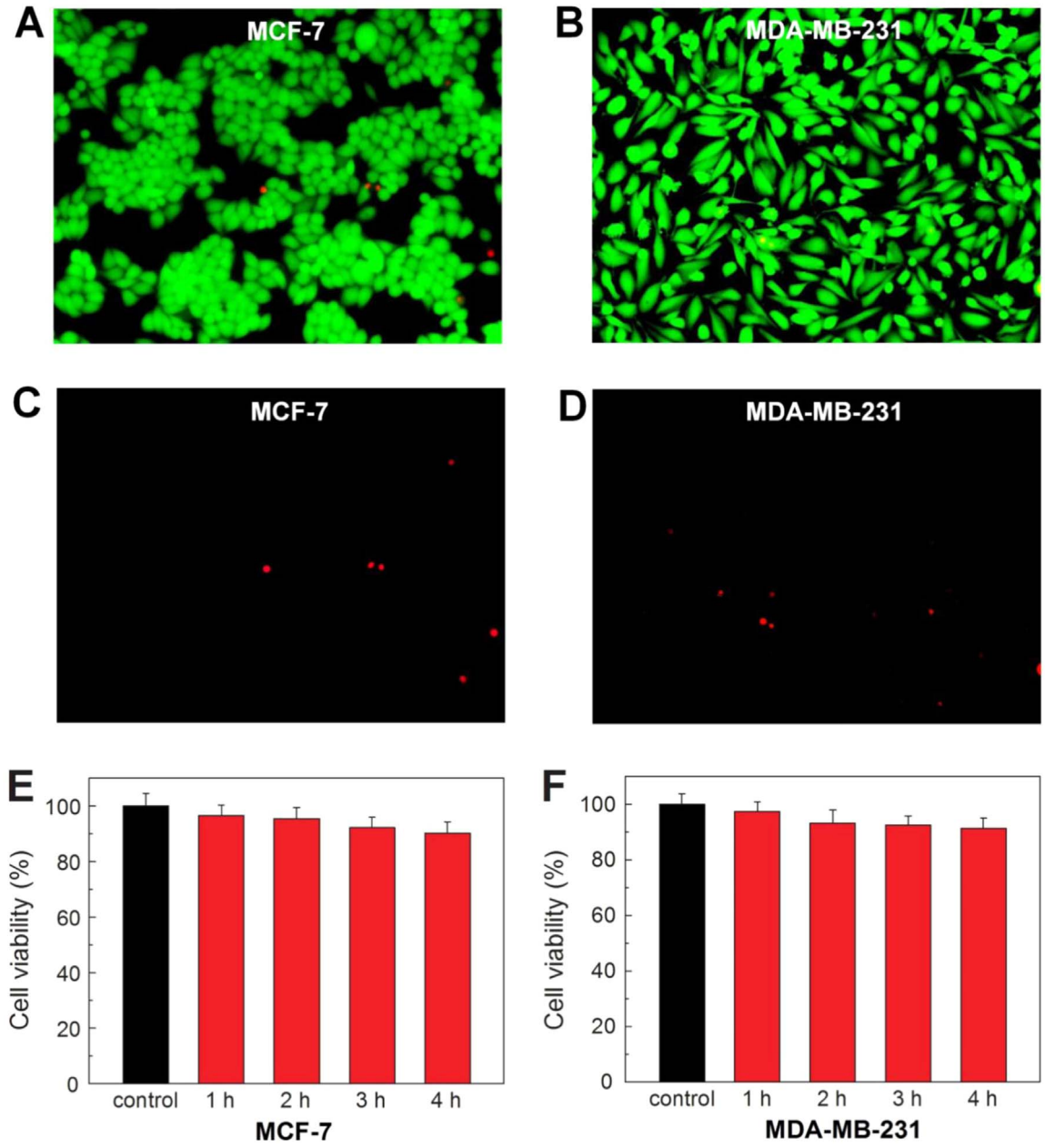

Fig. 5. (A)-(D) Live-dead fluorescent images of MCF-7 and MDA-MB-231 cells by calceinAM/PI assay to stain the viable cells green by calcein-AM and dead cells red by PI. (E) and (F) Quantitative cell viability results by CCK-8 assay for different cancer cells attached to and incubated with CF@NCNTAs–GNPs microelectrode for 0 h (control), 1 h, 2 h, 3 h and 4 h.

ratio of 80 and 43 for MCF-7 cells and MDA-MB-231 cells, respectively. Furthermore, the CCK-8 assay shows that MCF-7 cells maintain 96.6%, 95.4%, 92.1% and 90.2% cell viability after incubated with CF@NCNTAs–GNPs for 1 h, 2 h, 3 h and 4 h, respectively (Fig. 5E), and MDA-MB-231 cells maintain 97.5%, 93.2%, 92.6% and 91.3% cell viability after incubated with CF@NCNTAs–GNPs for 1 h, 2 h, 3 h and 4 h, respectively (Fig. 5F). These results demonstrate that CF@NCNTAs–GNPs possesses good biocompatibility to live cells, which is suitable for *in situ* real-time analysis in live cell samples.

The electrochemical detection of H_2O_2 secreted from live cancer cells was performed using CF@NCNTAs–GNPs microelectrode as the working electrode, where the fiber microelectrode was carefully located near the cells by a micromanipulator under the microscope in order to achieve the high sensitivity and accuracy (Fig. 6A). Herein, fMLP was selected as a stimulator to irritate the cells to exude H_2O_2 by disrupting intracellular redox homeostasis. As shown in Fig. 6B, after adding 0.1 mM fMLP, the amperometric current densities increase by 0.229 μA cm^{-2} and 0.189 μA cm^{-2} in testing solutions containing breast cancer cell lines MCF-7 cells and MDA-MB-231 cells, respectively, and both of which gradually decrease to background level when adding H_2O_2 scavenger (*i.e.,* catalase) into the testing solutions. However, the control experiment shows that the addition of either fMLP or catalase dose not generated any detectable amperometric signal in testing solution in the absence of live cells. These phenomena collectively indicate that the increased amperometric current originates from H_2O_2 secreted by live cells under the stimulation. The secreted amount of H_2O_2 from live cells can be calculated according to the sensitivity of CF@NCNTAs–GNPs microelectrode to H_2O_2 (*i.e.,* 142 μA cm^{-2} mM^{-1}), which is 1.61 μM for 5.0×10^6 MCF-7 cells and 1.33 μM for 5.0×10^6 MDA-MB-231 cells. Significantly, the secreted amount of H_2O_2 varies from different types of breast cancer cells. Therefore, the secreted amount of H_2O_2 form different live cells provides important information to investigate the oxidative stress capability in these cells, which offer the possibility to identify different types of cancer cells by

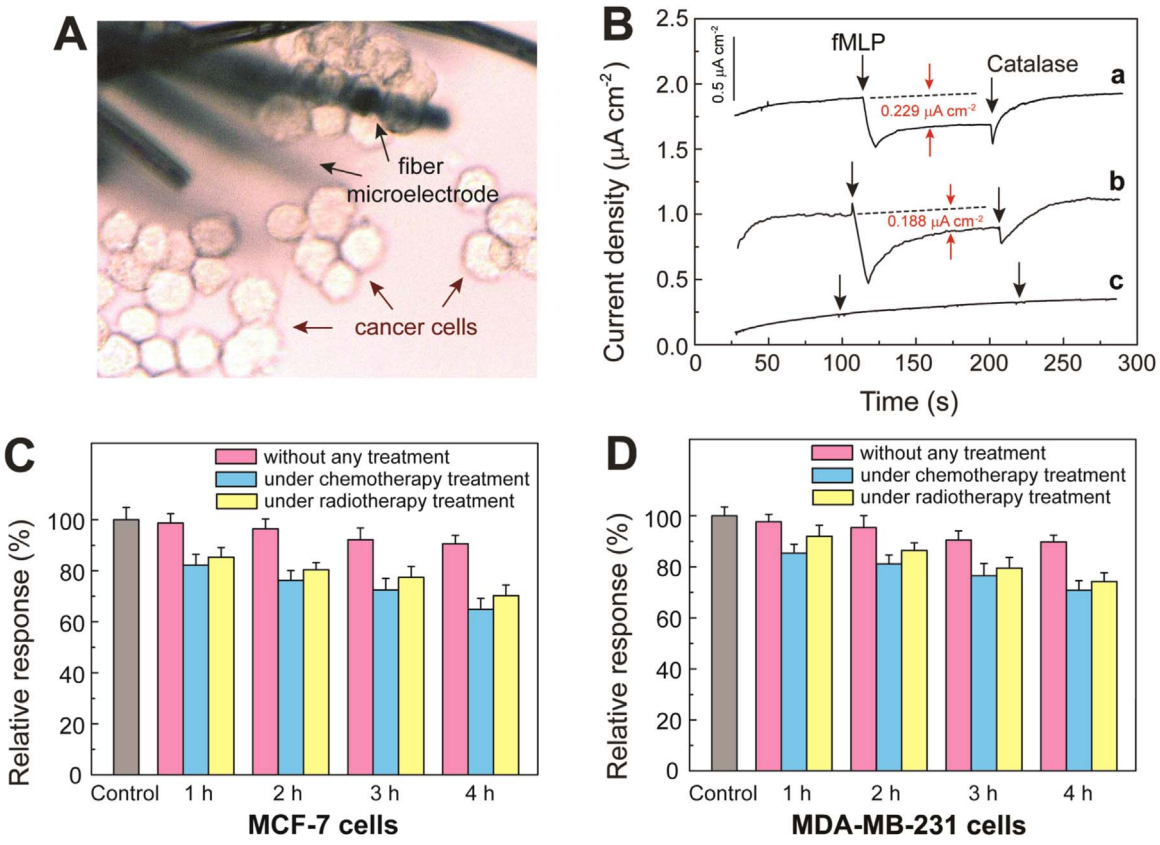

Fig. 6. (A) Super resolution digital microscope images of CF@NCNTAs–GNPs microelectrode located near the cells by a micromanipulator. (B) Amperometric current responses of CF@NCNTAs–GNPs microelectrode to the addition of 0.1 mM fMLP and 500 U mL^{-1} catalase in tested solution containing 5.0 × 10^6 MCF-7 cells (a), 5.0 × 10^6 MDA-MB-231 cells (b) and in the absence of cells (c). Histograms of the relative increased amperometric current responses of the secreted H_2O_2 from (C) MCF-7 cells and (D) MDA-MB-231 cells when it is 1 h, 2 h, 3 h and 4 h after chemotherapy or radiotherapy and without any treatment.

estimating their extracellular H_2O_2 level.

Furthermore, we have developed an electrochemical sensing platform to evaluate the sensitivity of different cancer cells to chemotherapy and radiotherapy. For chemotherapy testing, the breast cancer cells MCF-7 and MDA-MB-231 were treated with clinically anticancer drug cis-platinum (DDP). For radiotherapy treatment, the live cells were irradiated by 6 MV X-ray beams. Then the increased amperometric current responses of CF@NCNTAs–GNPs microelectrode to the stimulation of cancer cells by fMLP were recorded at a certain time after the treatments. As shown in Fig. 6C, the relative increased amperometric current responses to the stimulation of MCF-7 cells decline from 100% to 82.2%, 76.2%. 72.5% and 64.8% when it is 1 h, 2 h, 3 h and 4 h after DDP treatment, respectively, which are 85.3%, 80.4%, 77.4% and 70.2% at the same time after X-ray beam irritation. Nevertheless, the relative responses show a slight decrease from 100% to 98.8%, 96.4%, 92.3% and 90.6% for MCF-7 cells under the same condition but without any treatment. The RSD values are from 2.9% to 4.6%. These are due to the fact that treating cancer cells by chemotherapeutic agent or exposing cancer cells to X-ray beam will trigger cell death, leading to less amount of H_2O_2 released from cells upon simulation along with the time after chemotherapy or radiotherapy treatments. This trend has also been observed for MDA-MB-231 cells. The relative responses decline from 100% to 85.4%, 81.2%. 76.5% and 70.8% when it is 1 h, 2 h, 3 h and 4 h after DDP treatment, respectively, which are 92%, 86.4%, 79.5% and 74.2% at the same time after X-ray beam irritation. And without the treatment, the relative responses decrease from 100% to 97.7%, 95.4%, 90.5% and 89.8% for MDA-MB-231 cells under the same condition. The RSD values are from 2.6% to 4.8% (Fig. 6D). Evidently, MCF-7 cells are more sensitive to both chemotherapy and radiotherapy than MDA-MB-231 cells. This is of great significance for the development of effective therapy strategies in the treatment of different cancer diseases.

4. Conclusions

In summary, we have developed a new type of high-performance flexible nanohybrid microelectrode by taking advantage of unique features of different components in CF@NCNTAs–GNPs including: i) The robust CF offers the advantages of microscale size and mechanical flexibility, which serves as an ideal electrode substrate for sensitive *in situ* measurement. ii) The growth of highly ordered NCNTAs on CF dramatically increases its electrochemically active surface area and endows it with more active sites, which facilitate the further loading of functional nanomaterial on it. iii) The highly dense and uniformly dispersed GNPs decorated on NCNTAs support exhibit extraordinary electrocatalytic activity to the reduction reaction of H_2O_2. The nanohybrid fiber microelectrode integrates the mechanical, structural and electrochemical properties of different components in CF@NCNTAs–GNPs, and therefore demonstrates good sensing performance to H_2O_2 including low detection limit, wide linear range, high sensitivity and selectivity, exceptional mechanical stability and good biocompatibility, which enable it to be used in *in situ* real-time tracking H_2O_2 secreted from breast cancer cells, and evaluating the sensitivity of different cancer cells to chemotherapy or radiotherapy treatments. We envision our strategy of the design and construction of CF@NCNTAs–GNPs microelectrode would provide new insights on designing high-performance flexible fiber-based nanohybrid microelectrodes for *in situ* sensitive detection of biomarkers, which will contribute to the clinic diagnose and management of early-stage diseases.

Acknowledgements

This work is supported by National Natural Science Foundation of China (No. 51572094 and 51504168). We thank the Analytical and Testing Center of Huazhong University of Science and Technology, the Wuhan National Laboratory for Optoelectronics.

Appendix A. Supporting information

Supplementary data associated with this article can be found in the online version at http://dx.doi.org/10.1016/j.bios.2017.09.038.

References

Bai, J., Jiang, X., 2013. Anal. Chem. 85, 8095–8101.
Balamurugan, J., Thanh, T.D., Karthikeyan, G., Kim, N.H., Lee, J.H., 2017. Biosens. Bioelectron. 89, 970–977.
Beitollahi, H., Gholam, A., Ganjali, M.R., 2015. Mater. Sci. Eng. C-Mater. 57, 107–112.
Beitollahi, H., Tajik, S., Biparva, P., 2014. Measurement 56, 170–177.
Bojdi, M.K., Behbahani, M., Hesam, M., Mashhadizadeh, M.H., 2016a. RSC Adv. 6, 32374–32380.
Bojdi, M.K., Behbahani, M., Omidi, F., Hesam, G., 2016b. New J. Chem. 40, 4519–4527.
Bojdi, M.K., Mashhadizadeh, M.H., Behbahani, M., Farahani, A., Davarani, S.S.H., Bagheri, A., 2014. Electrochim. Acta 136, 59–65.
Chen, K.J., Chandrasekara Pillai, K., Rick, J., Pan, C.-J., Wang, S.H., Liu, C.C., Hwang, B.-J., 2012. Biosens. Bioelectron. 33, 120–127.
Chen, M., Tang, S., Guo, Z., Wang, X., Mo, S., Huang, X., Liu, G., Zheng, N., 2014a. Adv. Mater. 26, 8210–8216.
Chen, S., Hai, X., Chen, X.W., Wang, J.H., 2014b. Anal. Chem. 86, 6689–6694.
Chen, W., Yang, W., Lu, Y., Zhu, W., Chen, X., 2017. Anal. Chem. 9, 3213–3220.
Dong, S., Dao, A.Q., Zheng, B., Tan, Z., Fu, C., Liu, H., Xiao, F., 2015. Electrochim. Acta 152, 195–201.
Fang, X., Liu, J., Wang, J., Zhao, H., Ren, H., Li, Z., 2017. Biosens. Bioelectron. 97, 218–225.
Hossain, M., Luo, Y., Sun, Z., Wang, C., Zhang, M., Fu, H., Qiao, Y., Su, M., 2012. Biosens. Bioelectron. 38, 348–354.
Hosseini, H., Behbahani, M., Mahyari, M., Kazerooni, H., Bagheri, A., Shaabani, A., 2014. Biosens. Bioelectron. 59, 412–417.
Jayanthi, V.S.P.K., Sankara, A., Das, A.B., Saxena, U., 2017. Biosens. Bioelectron. 91, 15–23.
Ju, J., Chen, W., 2015. Anal. Chem. 87, 1903–1910.
Karimi-Maleh, H., Ensafi, A.A., Beitollahi, H., Nasiri, V., Khalilzadeh, M.A., Biparva, P., 2012. Ionics 18, 687–694.
Kim, T.H., Lee, D., Choi, J.W., 2017. Biosens. Bioelectron. 94, 485–499.
Lin, X., Ni, Y., Kokot, S., 2016. Biosens. Bioelectron. 79, 685–692.
Liu, J., Lu, L., Li, A., Tang, J., Wang, S., Xu, S., Wang, L., 2015. Biosens. Bioelectron. 68, 204–209.
Liu, R., Mahurin, S.M., Li, C., Unocic, R.R., Idrobo, J.C., Gao, H., Pennycook, S.J., Dai, S., 2011. Angew. Chem. Int. Ed. 50, 6799–6802.
Liu, W., Wang, H., Du, J., Jing, C., 2017a. Biosens. Bioelectron. 97, 70–74.
Liu, Y., Li, H., Guo, B., Wei, L., Chen, B., Zhang, Y., 2017b. Biosens. Bioelectron. 91, 734–740.
Mazloum-Ardakani, M., Ganjipour, B., Beitollahi, H., Amini, M.K., Mirkhalaf, F., Naeimi, H., Nejati-Barzoki, M., 2011. Electrochim. Acta 56, 9113–9120.
Mittal, S., Kaur, H., Gautam, N., Mantha, A.K., 2017. Biosens. Bioelectron. 88, 217–231.
Pan, L.H., Kuo, S.H., Lin, T.Y., Lin, C.W., Fang, P.Y., Yang, H.W., 2017. Biosens. Bioelectron. 89, 598–605.
Paul, K.B., Singh, V., Vanjari, S.R.K., Singh, S.G., 2017. Biosens. Bioelectron. 88, 144–152.
Prével, C., Pellerano, M., González-Vera, J.A., Henri, P., Meunier, L., Vollaire, J., Josserand, V., Morris, M.C., 2016. Biosens. Bioelectron. 85, 371–380.
Ravi, S.D., Iimura, K.I., Kato, T., 2003. Sens. Actuators B-Chem. 96, 523–526.
Rui, Q., Komori, K., Tian, Y., Liu, H., Luo, Y., Sakai, Y., 2010. Anal. Chim. Acta 670, 57–62.
Sun, Y., He, K., Zhang, Z., Zhou, A., Duan, H., 2015. Biosens. Bioelectron. 68, 358–364.
Sun, Y., Zheng, H., Wang, C., Yang, M., Zhou, A., Duan, H., 2016. Nanoscale 8, 1523–1534.
Taleat, Z., Mazloum-Ardakani, M., Naeimi, H., Beitollahi, H., Nejati, M., Reza-Zare, H., 2008. Anal. Sci. 24, 1039–1044.
Thanh, T.D., Balamurugan, J., Lee, S.H., Kim, N.H., Lee, J.H., 2016. Biosens. Bioelectron. 85, 669–678.
Wang, L., Dong, Y., Zhang, Y., Zhang, Z., Chi, K., Yuan, H., Zhao, A., Ren, J., Xiao, F., Wang, S., 2016a. NPG Asia Mater. 8, e337.
Wang, Y., Yu, L., Lou, X.W., 2016b. Angew. Chem. Int. Ed. 55, 14668–14672.
Wang, L., Xiong, Q., Xiao, F., Duan, H., 2017. Biosens. Bioelectron. 89, 136–151.
Xi, J., Xie, C., Zhang, Y., Wang, L., Xiao, J., Duan, X., Ren, J., Xiao, F., Wang, S., 2016. ACS Appl. Mater. Interfaces 8, 22563–22573.
Xi, J., Zhang, Y., Wang, N., Wang, L., Zhang, Z., Xiao, F., Wang, S., 2015. ACS Appl. Mater. Interfaces 7, 5583–5590.
Xiao, F., Li, Y., Gao, H., Ge, S., Duan, H., 2013. Biosens. Bioelectron. 41, 417–423.
Xiao, F., Song, J., Gao, H., Zan, X., Xu, R., Duan, H., 2012. ACS Nano 6, 100–110.
Xu, P., Wang, K., Lu, C., Dong, L., Gao, L., Yan, M., Aibai, S., Liu, X., 2016. J. Ethnopharmacol. 193, 408–415.
Yang, B., Zhang, Y., Chen, B., He, M., Yin, X., Wang, H., Li, X., Hu, B., 2017. Biosens. Bioelectron. 96, 77–83.
Yu, X., Fan, H., Wang, L., Jin, Z., 2014. Angew. Chem. Int. Ed. 53, 12600–12604.
Zhang, Y., Bai, X., Wang, X., Shiu, K.K., Zhu, Y., Jiang, H., 2014. Anal. Chem. 86, 9459–9465.
Zhang, Y., Bo, X., Nsabimana, A., Munyentwali, A., Han, C., Li, M., Guo, L., 2015. Biosens. Bioelectron. 66, 191–197.
Zhong, S.L., Zhuang, J., Yang, D.P., Tang, D., 2017. Biosens. Bioelectron. 96, 26–32.
Zhu, L., Zhang, Y., Xu, P., Wen, W., Li, X., Xu, J., 2016. Biosens. Bioelectron. 80, 601–606.
Zhuang, Z., Sheng, W., Yan, Y., 2014. Adv. Mater. 26, 3950–3955.